Precision Engineering 91 (2024) 489–498

Contents lists available at ScienceDirect

Precision Engineering

journal homepage: www.elsevier.com/locate/precision

Deformation and optical aberration prediction in ultra-precision Single Point Diamond Turning of optical components

Daniele Gottini [a,*], Giovanni Scimia [b], Niccolò Grossi [a], Antonio Scippa [a]

[a] Department of Industrial Engineering, University of Florence, Via di Santa Marta 3, 50139, Firenze, Italy
[b] Leonardo Electronics, Via delle Officine Galileo, 1 – Campi, Bisenzio, 50013, Italy

ARTICLE INFO

Handling Editor: Dr. Masonori Kunieda

Keywords:
Single point diamond turning
Mirror
Aluminum
Deformation
Zernike

ABSTRACT

Aluminum is the material of choice for the majority of aerospace components, and, in the past few years, its application has been extended also to the mirrors of space telescopes because of the improved thermal behavior and the possibility to build the entire telescope with the same material. However, the low elastic modulus of such material, combined with the extremely tight tolerances of optical applications, make the production of these components very challenging and, usually, based on a trial-and-error approach. This paper presents a structured methodology for the prediction of the results of manufacturing in Single Point Diamond Turning of optical components, both in terms of absolute deformation as well as optical aberrations (via Zernike polynomials). All the most significant parameters acting on the workpiece have been simulated and combined. The proposed approach has been experimental validated on an actual aluminum mirror, proving its good accuracy (<5 % rms error). While some improvement can be performed to better match the experimental data in terms of Zernike coefficients, especially for non-symmetric aberrations, this paper forms the basis for an off-machine optimization of the SPDT process, drastically reducing the trial-and-error efforts.

1. Introduction

Mirrors are the main component of the majority of space telescopes. They combine the stringent mass and stiffness requirements typical of space components, with the extreme requirements in terms of surface finish needed for optical performance. This poses challenges in both their design and optimization for operating performances, as well as their manufacturing.

The production of such components is usually comprised of three main phases, sometimes interspersed by thermal treatments: i) rough traditional machining, ii) ultra-precision machining, iii) post-polishing.

The latter is a very slow process in which the removal rate is extremely low (tenths of micron per minute) [1,2], thus requiring starting surface errors in the order of microns. For this reason, it is critical to reduce as much as possible the surface errors coming from the previous phase (ultra-precision machining).

Single Point Diamond Turning (SPDT) is one of the most used ultra-precision machining processes, it is especially indicated for axial-symmetric surfaces, which characterize most mirrors' reflective surfaces. Such process is an analogue to traditional turning, using a very small diamond tool and extremely precise machine tools. Using this process, it is possible to obtain excellent surface finishes, with roughness in the order of 1 ÷ 10 nm and shape error below 100 nm RMS [3–6], especially when working on Nickel-plated mirrors.

Steadily increasing interest is being put in the development of fully metallic mirrors due to their easier machinability, improved thermal behavior and lower cost with respect to vitreous ones [7], as well as the possibility to build the entire telescope with the same material [8].

A typical material of choice for these kinds of mirrors is Aluminum, which poses several advantages in the operative phase. It, however, comes with the downside of being a very soft material and, thus, very susceptible to deformations. For this reason, aluminum mirrors are especially critical when it comes to manufacturing since even small loads may induce unacceptable deformation of the reflective surface. To mitigate this problem, the tuning process is based on a trial-and-error approach, resulting in a large number of reworks of both the workpiece and the fixture: this implies longer lead time and lower asset availability for production.

In order to reduce the number of iterations and discard, in the design phase, design-process combinations that are not advantageous, it would be extremely convenient to make use of predictive models able to simulate the result of manufacturing, in the same way as what is done for

* Corresponding author.
E-mail address: daniele.gottini@unifi.it (D. Gottini).

https://doi.org/10.1016/j.precisioneng.2024.10.010
Received 17 July 2024; Received in revised form 2 October 2024; Accepted 15 October 2024
Available online 18 October 2024

other machining processes [9,10]. Regarding this, only a few solutions have been proposed in literature for SPDT, and all limited to some specific aspects.

Focusing on cutting forces in SPDT, Huang and Lee estimated and evaluated their relationship with the cutting parameters [11] while Dai et al. related such forces with misalignments of the cutting tool [12]. Both studies showed that, for standard cutting parameters (1 ÷ 10 μm depth of cut, feed rate <30 mm/min), such forces are in the order of some tenths of N and, thus, negligeable for what regards the deformations they induce on the reflective surface during the machining.

Gerchman analyzed the well-known ogive effect caused by a tool misalignment [13], which results in a variation of radius of curvature of the final piece. This effect is usually compensated after the 1st machining of the workpiece by measuring the surface and correct the misalignment.

The centrifugal force acting on a machined workpiece during SPDT has been evaluated by Zhang et al. [14]. In their study they minimized such effect by reducing the spindle speed and inserting in the system multiple support points. While the reduction in rotational speed is a generally applicable result, with a lower limit imposed by the surface quality of precision optics, the increase of supporting points is very case dependent and requires additional investigation.

Several studies have been conducted on the effect of fixturing on the machining of flexible components [15–19], but only few analyze SPDT in detail, focusing on the enhancement of fixturing [20–22].Although a thorough analysis of the effect that fixtures on SPDT have on the surface finish of a mirror is missing, some studies were carried out on the errors induced by screw tightening and mounting operations on the reflective surfaces under operating conditions [23,24].

However, a comprehensive approach that combines all the main aspects, and thus able to effectively predict the manufacturing errors during SPDT of flexible structures made of soft materials (like aluminum), has not yet been proposed.

In addition to that, the main optical requirement for a mirror is usually not expressed in terms of overall deformation of the surface, but in terms of optical aberrations. For this reason, in order to evaluate the quality of a reflective surface, an optical performance analysis of such surface is needed.

The most widely spread optical analysis is the decomposition in Zernike polynomials, which aims to fit the deformed shape of a reflective surface with a linear combination of analytical contributions [25,26]. Such analysis is particularly useful when comparing numerical results with experimental data obtained via interferometry as, in interferometric measurements, the measured component is placed at a certain distance from the illuminator-detector in such a way that the image is focused [27]. In terms of Zernike polynomials, this means that not only the rigid body motion components of the measured surface are inherently subtracted from the measurement, but also the defocusing (4th Zernike polynomial in the Noll sequence [26]) does not appear in the measurement.

Despite the importance of such analysis, no study in literature involving the manufacturing of optical components considers this aspect of the deformations induced on the surface.

The scope of this work is to present a structured, comprehensive methodology for the prediction of manufacturing errors in SPDT. Such methodology exploits FEM simulations and shows how to take into account of the primary factors, and their interactions, in order to obtain an accurate prediction both in terms of mechanical deformations as well as optical aberrations.

In particular, the presented methodology considers and combines the following parameters: tool misalignment errors, gravity, centrifugal force, fixturing, while neglecting some secondary effects such as cutting forces, aerodynamic forces and tool wear.

In order to better characterize the errors induced on the reflective surface from an optical point of view, a Zernike decomposition of the predicted results of manufacturing completes the methodology, allowing to directly relate to specific optical requirements.

In section 2, the proposed methodology is explained. It is then applied on a case study, presented in section 3, and the results of the approach, as well as their validation with experimental data, are shown in section 4.

2. Proposed methodology

The proposed approach involves a FEM-based predictive model of the SPDT process, that requires to take into account of the various loads and constraints acting on the workpiece, the possible errors induced by imperfections in the machining setup and their combination with the behavior of not only the workpiece, but also all the support equipment (i.e., fixturing) used in the process.

As already highlighted in the introduction, literature shows how the most significant parameters are the following.

1. Gravity
2. Centrifugal force
3. Tool misalignment errors
4. Fixturing

Such parameters are included in the proposed methodology while other parameters have instead been neglected such as cutting forces, aerodynamic forces, residual stress released during machining, thermal effects and shocks generated by intermittent cutting.

As highlighted by literature [11,12] cutting forces acting on the workpiece during SPDT are in the order of few tenths of Newtons for most applications. They may be relevant for some very specific case, but not in general and are neglected in this approach.

The rotation of the workpiece and its supports may generate some aerodynamic forces on the system. However, they are extremely case dependent and, for most geometries and at the low spindle speed usually used in SPDT, such forces can be neglected [28].

Another significant source of distortion is residual stresses that can be relieved during machining. However, since to avoid such error, ultra-precision machining is generally performed after a dedicated heat treatment phase, this phenomenon is neglected in this work.

Under these hypotheses, the methodology explained in this paper follows the scheme in Fig. 1.

The proposed methodology involves the development of a finite element model of the workpiece and support assembly. Such model is used to perform, separately, simulations for centrifugal force, gravity and fixturing. Those analyses are then post-processed and combined with each other as well as with a model representing alignment errors.

The various contributions and their implementation in the proposed methodology, are explained more in detail in the next subsections.

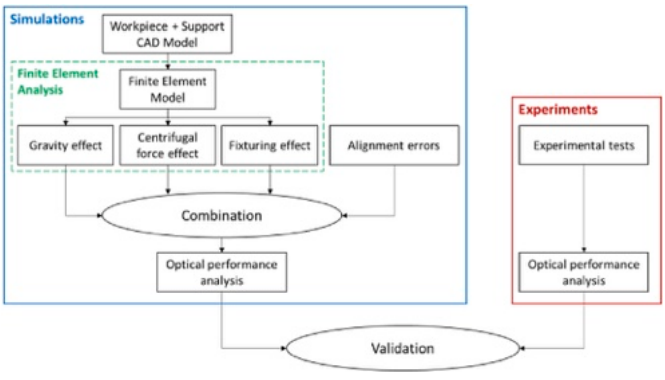

Fig. 1. General overview of the predictive algorithm.

2.1. Centrifugal force

The centrifugal force is a body force acting radially on the workpiece because of spindle rotation. In case of constant angular velocity, such force can be simulated as a constant radial body force (e.g., RFORCE in MSC Nastran).

2.2. Gravity acceleration

During the turning operation, the direction of gravity acceleration varies with respect to a reference frame integral with the workpiece. Depending on the tool feed direction, however, it is possible to relate the direction of gravity in the instant in which a point is being machined, with the position of said point. For example, in case of horizontal tool feed direction, the direction of the gravity acceleration will always be orthogonal to a line connecting the machined point with the axis of rotation (Fig. 2). Exploiting this property, it is possible to obtain the surface error induced by gravity by combining only two simulations (one with gravity acting along x and one acting along y).

The resulting deformation will be, for each node, the sum of the displacement of that node caused by gravity along x, multiplied by an appropriate scaling factor, plus that of the same node caused by gravity along y, scaled by another appropriate factor (Equation (1)).

$$dz_i = v_{i_x} * dz_i|_{g_x} + v_{i_y} * dz_i|_{g_y} \tag{1}$$

Where dz_i is the Z displacement induced by gravity on the i^{th} node, $v_i = \begin{bmatrix} v_{i_x} \\ v_{i_y} \end{bmatrix}$ is the unit vector of the node position and $dz_i|_{g_x}$ and $dz_i|_y$ are the Z displacements of the i^{th} node calculated, respectively, in the case of gravity along x and gravity along y.

2.3. Fixturing

Fixturing proved to be an issue for what regards optical surface performances. One example of deformations induced by the fixturing to the reflective surface of a mirror can be found in Ref. [9]. Moreover, fixturing components in the manufacturing phase are generally different from the ones used during the operating life of the mirror. It is thus important to include such contribution to any predictive algorithm.

Some solutions traditionally selected to solve this problem involve.

- Avoiding, everywhere possible, the use of screws for mirrors' junctions;
- Where unavoidable, reduce as much as possible the preload of the screws;
- Increase the stiffness of supporting equipment.

These solutions, however, are usually achieved by trial and error. For this reason, they are extremely case-dependent and cannot be easily generalized.

In order to simulate effects related to screw tightening, the methodology described in this paper prescribes (see Fig. 3).

- Modelling of the thread in socket with rigid beam elements connecting all the nodes of the gripping area with a node on the hole axis at 1/3 of the gripping area length
- Modelling of the head of the screw with rigid beam elements connecting all the nodes of the contact zone between piece and screw's head, with a node at the intersection between the contact plane and the hole axis
- Modelling of the contact zones between the connected pieces with rigid beam elements connecting all the nodes of an area surrounding the screw hole, of dimensions representative of the connection's pressure cone, with a node at the intersection between the contact plane and the hole axis
- Approximation of the screws behavior with flexible elements between pivot nodes of the contact zones on the two connected pieces
- Preload forces applied to the pivot nodes of rigid beam elements, perfectly aligned, opposite in direction but equal in modulus.

This connection scheme meant to represent the stress distribution inside the screws as described in the ECSS standards [29] as well adopted in other works [30].

2.4. Tool misalignment

As introduced in section 1, a tool misalignment causes a shape error of the manufactured piece. This effect, in case of spherical surfaces, is well approximated by an ogive. A simplified model of such effect is shown in Fig. 4. This effect can be represented, as explained in Ref. [13], by the following equation (see Fig. 5).

$$z = r - \sqrt{r^2 - \left[(\rho^2 - \delta y^2)^{\frac{1}{2}} - \delta x\right]^2} \tag{2}$$

Where ρ is the distance of the tool from the spindle rotation axis, δx and

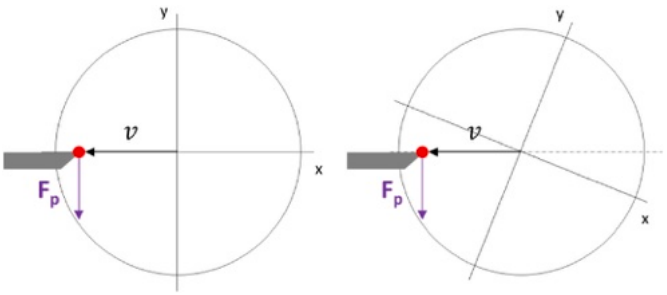

Fig. 2. Gravity acceleration.

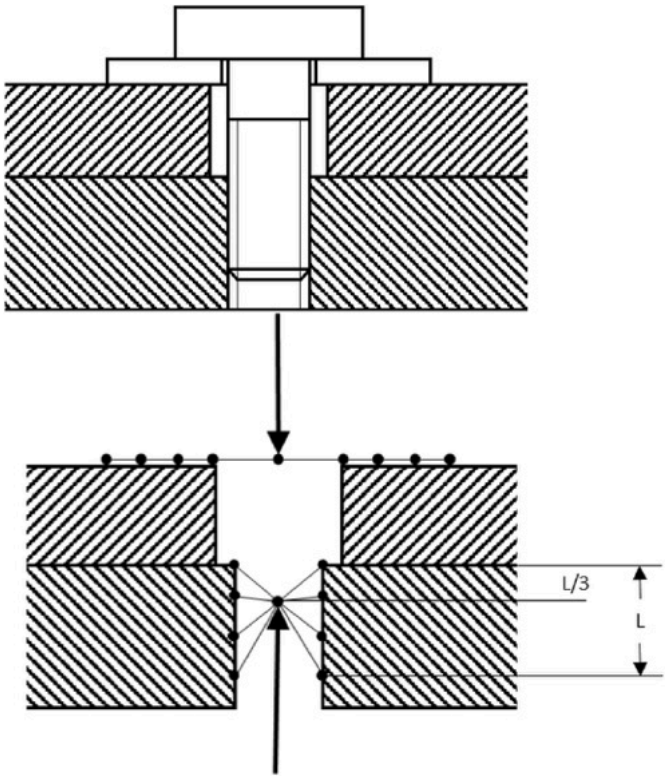

Fig. 3. Modelling of screw tightening.

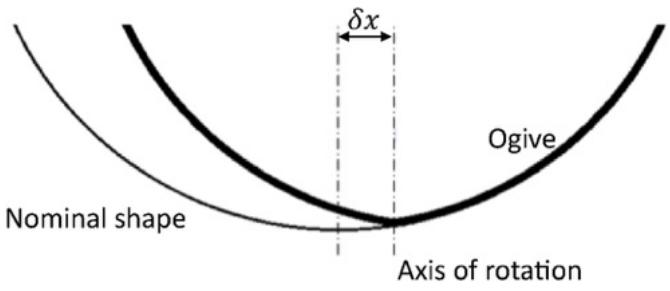

Fig. 4. Ogive effect.

δy are the tool misalignments in the x and y direction, and r is the nominal curvature radius of the sphere to be machined.

Approximated versions of this formula are widely used to correct misalignment errors in SPDT generated mirrors. In this paper, however, we suggest using the more general one, as it can be applied to a wider variety of cases.

Note that the ogive effect is extremely unpredictable, therefore, tool misalignments (i.e., δx, δy) are easier to be estimated with an interferometric measurement of the workpiece after the 1st turning and use the algorithm (i.e., eq. (2)) to correct it on the following passes.

2.5. Optical performance

As mentioned in the introduction, in order to define the quality of the reflective surface of a mirror, such surface has to be evaluated in terms of optical performance. This remains true also when trying to predict the quality of the workpiece produced.

In the proposed methodology the deformed shape of the surface, simulated as discussed in the previous sections, is then fitted using the Zernike polynomials [26]. This way it is possible to predict the outcome of the manufacturing process, not only in terms of overall deformation, but also in terms of optical aberrations and, thus, evaluate if the final shape meets the requirements for each specific aberration term. Table 1 shows the first 15 aberrations in the Noll index [26].

3. Experimental validation

The proposed methodology was applied on a specific case study and subject to experimental validation to assess its accuracy and effectiveness.(See Fig. 5)

3.1. Case study

The workpiece shown in figure represents the one used in the above-mentioned case study.

Table 1
Optical aberrations, Noll index.

Order	Noll Index	Aberration
0th	1	Piston
1st	2	Tip
	3	Tilt
2nd	4	Defocus
	5	Oblique Astigmatism
	6	Vertical Astigmatism
3rd	7	Vertical Coma
	8	Horizontal Coma
	9	Vertical Trefoil
	10	Oblique Trefoil
4th	11	Primary spheric
	12	Secondary vertical astigmatism
	13	Secondary oblique astigmatism
	14	Vertical Quadrafoil
	15	Oblique Quadrafoil

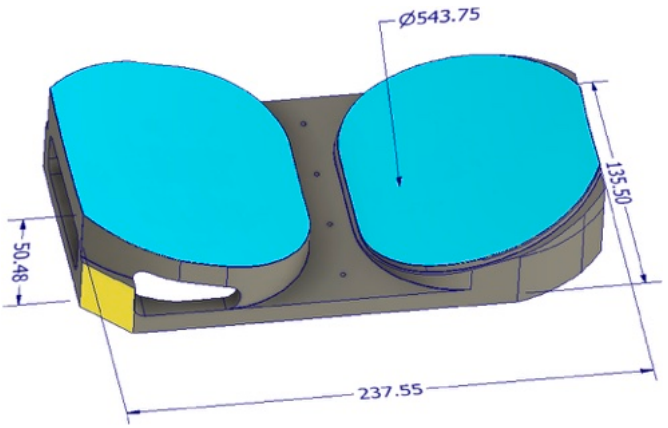

Fig. 5. Case study, workpiece.

Such component is a monolithic piece made of aluminum of the Al6xxx series in which two spherical mirrors are built on the same substrate (similarly to the case study presented in Ref. [31]). The spherical mirror analyzed in this paper is characterized by a diameter of 543.75 mm. Overall dimensions of the workpiece are 135.50 x 237.55 × 50.48 mm. It is mounted on the SPDT machine with a set of support equipment. Fig. 6 shows a CAD model of the assembly. The various components, numbered in the figure, are listed below.

1. The workpiece
2. A custom service plate made of the same material of the workpiece
3. Seven cylindrical spacers
4. Two counterweights connected to the service plate with M4 steel screws
5. M3 steel grains connect the spacers to the workpiece
6. M3 steel screws connect the spacers to the service plate

The tungsten counterweights are so that not only the center of mass of the assembly falls on the spindle axis, but also one of the principal inertial directions coincide with that axis. This way the assembly is balanced. Only three of the seven spacers (in blue in figure) are tightened to the service plate, while the others are just touching. The service plate is connected to the spindle of the SPDT machine on the back side, with pneumatic depression.

For the experimental validation, the workpiece was machined with a single point diamond tool with depth of cut (P) and feed (F) set according to the tool manufacturer suggested parameters (P 1–5 μm, F 5–15 μm/revolution). Before performing SPDT the workpiece residual stresses were relieved through a dedicated heat treatment procedure.

After SPDT, deformations of the reflective surface have been

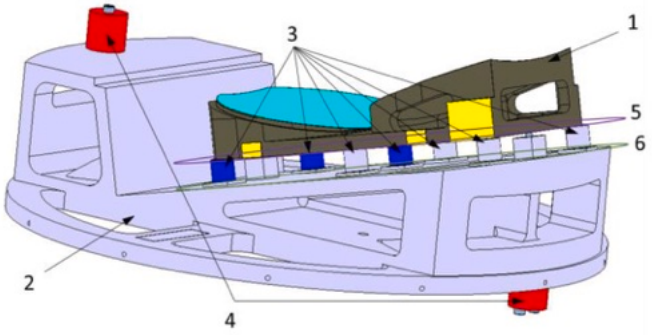

Fig. 6. Case study, assembly: 1) Workpiece, 2) Service Plate, 3) Spacers, 4) Counterweights, 5) M3 grains, 6) M3 steel screws.

measured using an interferometer. To do so, an illuminator is placed on the focus of the mirror and then measurements are taken. By doing so, rigid body motions of the surface, as well as defocusing components, do not appear in the measured deformed shape [32].

3.2. Implementation of the proposed methodology

In order to apply the proposed methodology, the case study has been modelled via Finite Element Method (FEM), MSC Nastran solver was used to perform the analysis. Following the procedure described in section 2.

1. The geometry was simplified and meshed with 2nd order tetrahedral solid elements (see Fig. 7). The tungsten counterweights have been approximated by two point-masses (CONM2 in Nastran) connected to all the nodes of the contact region between the counterweights and the service plate via rigid elements (RBE2 in Nastran).
2. The fastened connections between the various components have been modelled with MPC elements (RBE3 in Nastran) connecting all the nodes in the interface region to a pivot placed at the intersection between the axis of the screw/grain and the interface plane. The pivots of the two surfaces in contact have been then connected with flexible elements (CBUSH in Nastran) having the stiffness properties (typical for steel screws) shown in Table 2(see Fig. 8).
3. The connection with the spindle has been represented with single point constraints (SPC in Nastran) in the contact region between the service plate and the spindle (Fig. 9): the nodes on the border are restrained in X and Y directions (red and green arrows in coordinate system B in Fig. 10), while all the nodes inside the region are restrained in Z (blue arrow in the same reference frame).
4. Two additional reference frames have been created: one with Z axis perpendicular to the interface plane between cylinders and service plate (A in Fig. 10); the other with Z axis coincident with the spindle axis (B in Fig. 10)

Following the prescriptions described in sections 2.1 to 2.4.

Fig. 7. Case study assembly FEM model.

Table 2
CBUSH properties.

Direction	Joint stiffness	
	Translation Stiffness	Rotation Stiffness
In-plane	1.0 E10 N/m	1.00 E8 (N m)/rad
Axial	1.0 E10 N/m	1.00 E8 (N m)/rad

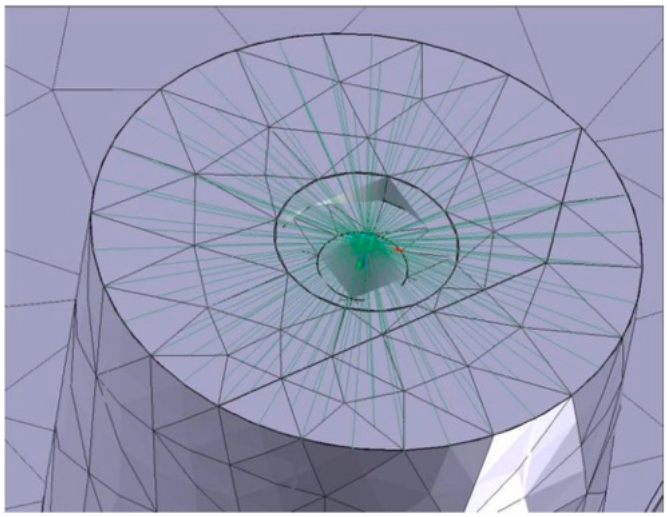

Fig. 8. Fastened connections modelling.

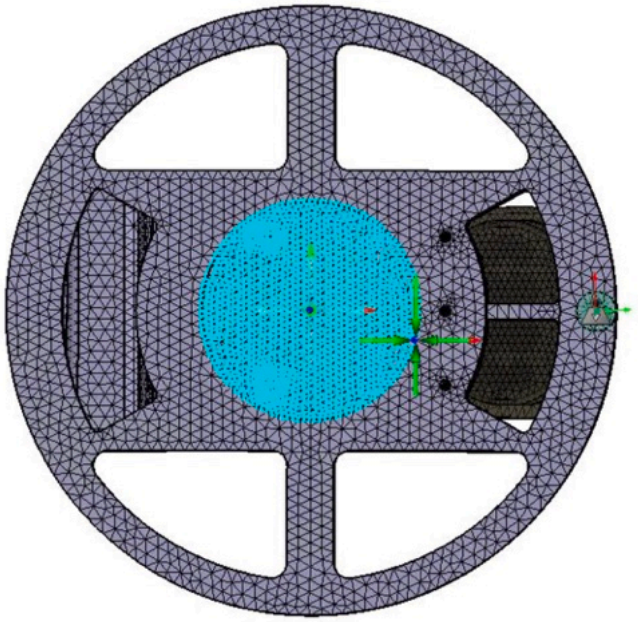

Fig. 9. Model constraints.

- Gravity has been simulated with a body force (GRAV in Nastran). Two analyses were carried out for two different cases: gravity along X and gravity along Y of the Coordinate system labelled as “B” in Fig. 10.
- A radial body force (RFORCE in Nastran) has been used to simulate the centrifugal effect. Such force has been applied on the spindle rotation axis with a nominal spindle speed of 1 rpm.
- The preload of each loaded screw has been modelled with two opposite coaxial forces acting on the pivot points of the rigid

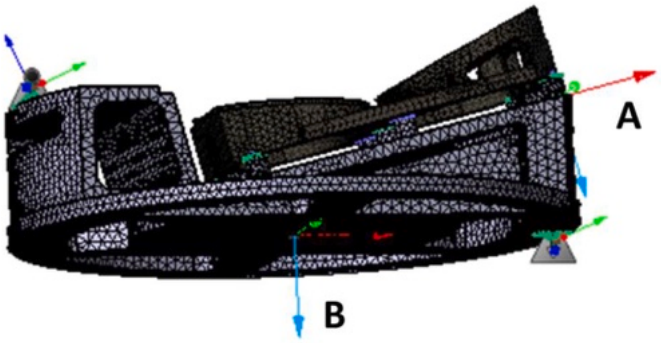

Fig. 10. Additional reference frames A and B.

elements (RBE3) representing screw head and thread for each joint. As in the real case study, only three of the seven spacers have been tightened (Fig. 11). For each force, a value of 1N was selected.

- The shape error caused by tool misalignment has been calibrated using the tests and resulted in a misalignment ($\delta x = \delta y$) of 10 μm. Such shape was simulated using equation (2) shown in section 2.4.

It is important to note that the various errors are obtained by linear analyses and can therefore be scaled and combined linearly.

All four contributions are linearly independent with each other, for this reason, each analysis was performed separately, with unit loads, and then the results were scaled and combined on a separate post-processing software (MathWorks Matlab).

4. Results and discussion

4.1. Numerical results

The results of the analyses, in terms of deformations of the reflective surface, are shown in Figs. 12–13-14-15. Note that components of rigid body motion of the surface are not relevant in terms of optical performance and have been, thus, removed from the results in order to show only the effective deformation of the surface.

Note that Figs. 12 and 14 show the deformation map induced by unitary load for, respectively, centrifugal force and screws preload. Such values are scalable for the actual ones used for the case study.

The surface error is evaluated in terms of root mean square (RMS) of the deformation. The deformation maps shown in Figs. 12-15 show that.

1. The ogive effect causes an axially symmetric error which is characterized, in terms of optical aberrations, by a significant defocusing component. Since the defocusing contribution is not interesting in

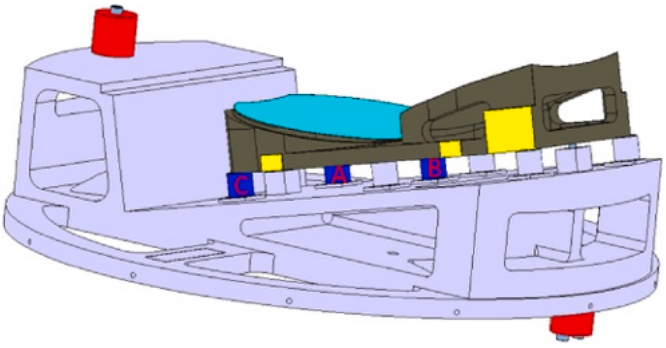

Fig. 11. CAD model of the case study. In blue, coded with A, B, C, the tightened cylinders. (For interpretation of the references to colour in this figure legend, the reader is referred to the Web version of this article.)

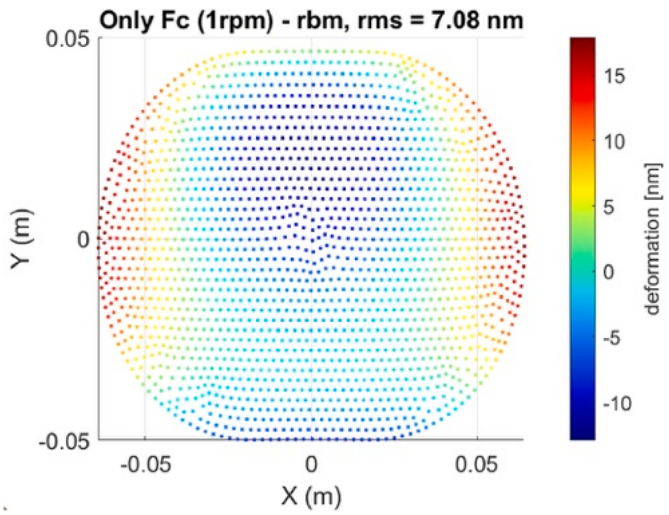

Fig. 12. Centrifugal forces, 1 rpm.

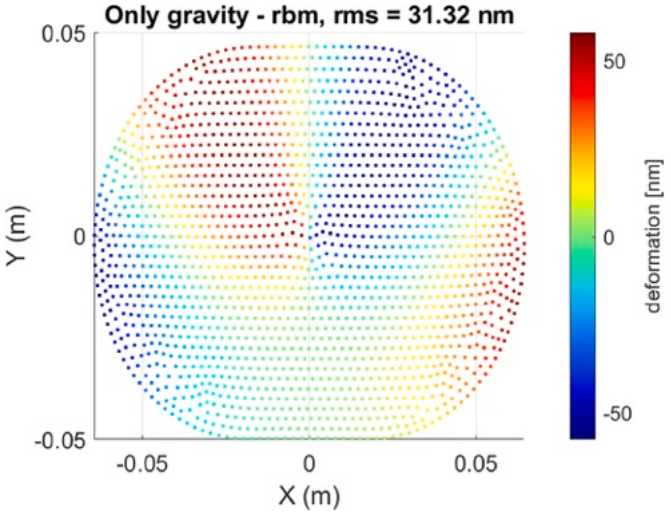

Fig. 13. Gravity.

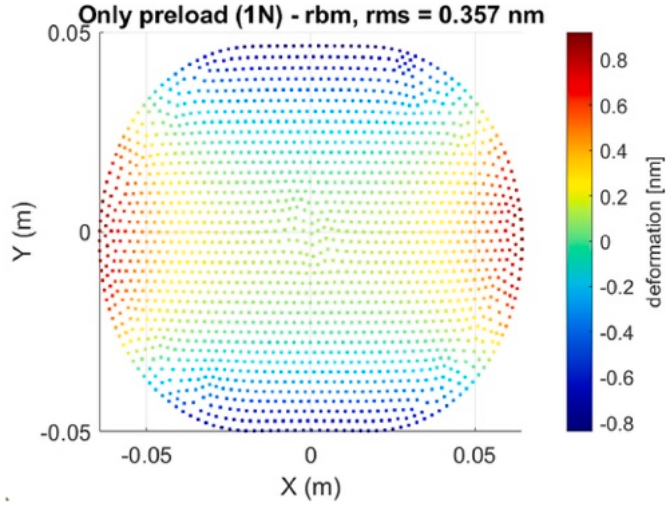

Fig. 14. Screws preload, 1 N.

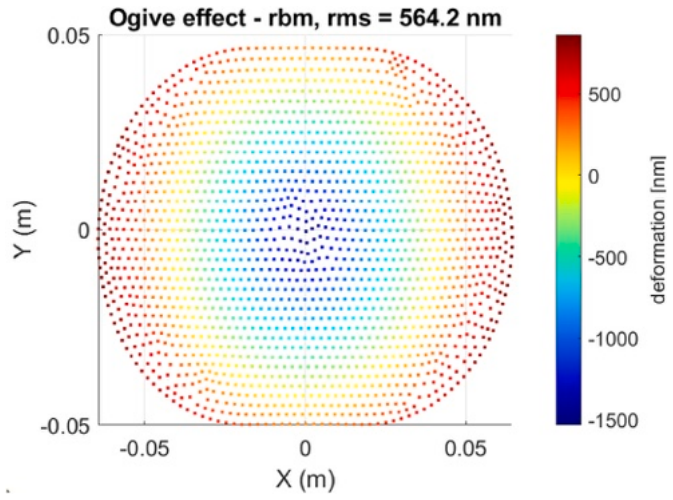

Fig. 15. Tool misalignment, $\delta x = \delta y = 10\,\mu m$.

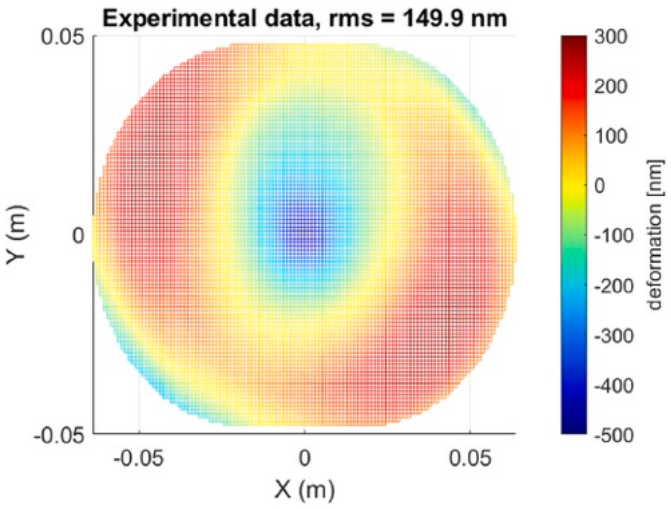

Fig. 16. Experimental results.

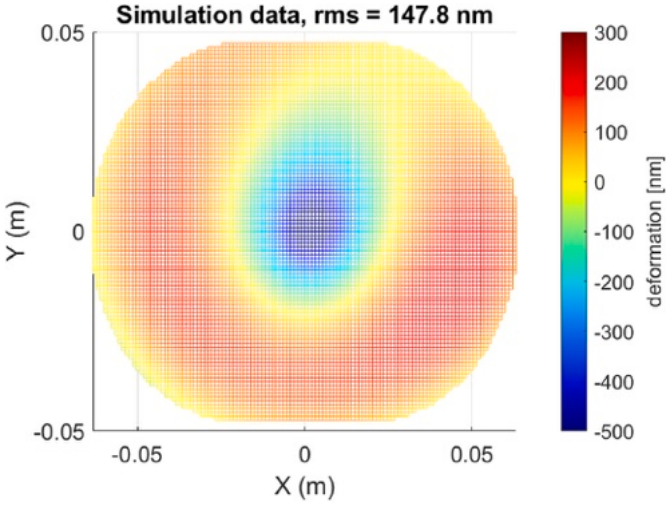

Fig. 17. Proposed methodology results.

terms of optical performance (see next section), a further manipulation of this effect is required once combined with the other errors.
2. The surface errors caused by centrifugal force and preload can be combined with all the other contributions by scaling them to the experiment value
3. The gravity effect provides a surface error of 31.32 nm RMS which is strongly anti-symmetric that can't be easily represented by a single optical aberration.

In order to combine the various contributions properly as well as to compare the numerical results with the experimental ones, some additional manipulation is required. In the following sections, an optical performance analysis procedure is explained and applied to the case study to perform a comparison between numerical and experimental data.

4.2. Experimental results

Case study has been manufactured and the reflective surface of the mirror has been measured directly on the machine, with the workpiece still mounted on the assembly. For this reason, the effect of the release of the screw tightening is not acting on the surface. Therefore, the numerical simulation to be compared with the experimental data is composed of.

- The effect of release of the stresses caused by the centrifugal force (Fc) (Fig. 12);
- The effect of release of the stresses caused by gravity (g) (Fig. 13);
- The ogive effect (ogive) (Fig. 15).

Which means that the map representing the machined surface (map_{tot}) will be equal to:

$$map_{tot} = -map_{Fc} - map_{g} + map_{ogive}$$

Where the various map_i are the map of the displacements caused by the i^{th} term. Note that, in the combination, the surface error related to the centrifugal force has been scaled to the experiment's spindle speed.

The measurement of the workpiece has been carried out using an interferometer, for this reason, the map obtained by combination of the simulated errors, needs to be truncated by the rigid body and defocusing components. As mentioned in the introduction, interferometric measurements inherently subtract rigid body motions and defocusing of the surface. A comparison of the simulated surface and the experimental one, after this post-processing, is shown in Figs. 16 and 17.

The comparison between the two maps in terms of maximum, minimum and root mean square (RMS) is shown in Table 3, while Figs. 18 and 19 show a section of the surface in X = 0 and Y = 0.

Such comparison show that the numerical model matches well with experimental data, proving the accuracy of the proposed methodology, in fact.

- The lowest point, caused by the ogive effect, is characterized by a very similar deformation, in the order of the tenth of micron of difference, in the two maps ("Min" column in Table 3)
- The two sections, x = 0 and y = 0, shown in Figs. 18 and 19, as well as the surface maps in Figs. 16 and 17, underline the overall good matching of the shape of predicted and experimental shapes.

Mirrors are usually subject to additional requirements in term of optical performance, asking to have RMS related to the nth Zernike

Table 3
Maximum, minimum and RMS comparison between experiment and simulation.

	Max [nm]	Min [nm]	RMS [nm]
Simulation	218	−647	147.8
Experiment	297	−485	149.9
Difference	**79.1**	**162**	**7.02**
% Difference	**36 %**	**25 %**	**1.4 %**

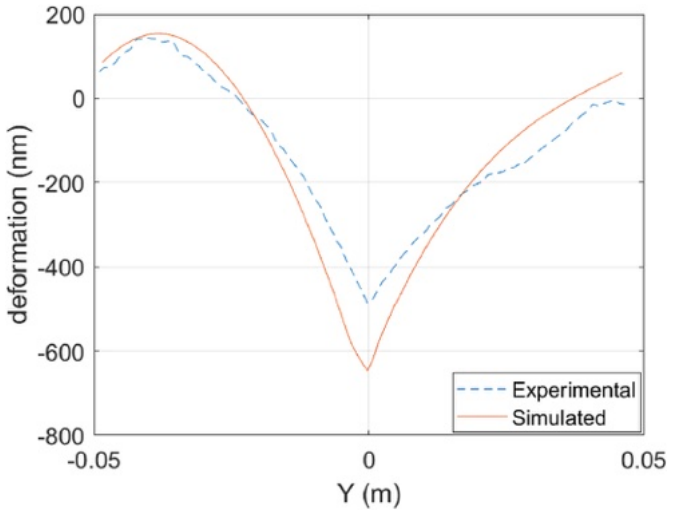

Fig. 18. Section at X = 0.

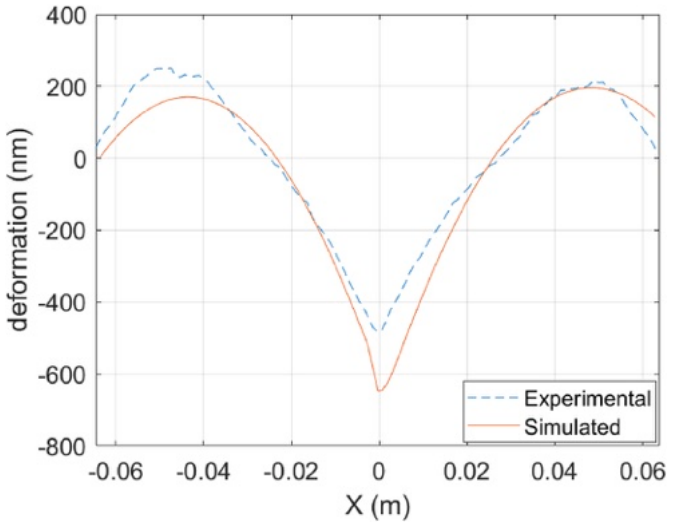

Fig. 19. Section at Y = 0.

polynomial below a certain value. The optical performance carried out on the case study made use of the first 15 Zernike polynomials (indexed following the Noll sequence), representing components up to the 4th order terms.

In histogram in Fig. 20 the first 15 Zernike polynomials for experimental (blue) and simulated (red) data. Fig. 20 underlines that experimental data are primarily characterized by astigmatism (5th and 6th coefficient), coma (7th coefficient) and 2nd order spheric (11th coefficient). The most significant of these is the spheric and such aberration is well fitted by the simulation (6 % error).

For what regards the other significant coefficients (5th, 6th and 7th), instead, they are not well represented. For this reason, if the aim is to evaluate the optical performance of the machined piece just by numerical simulations, some additional refinement has to be performed on the model.

4.3. Considerations on the tool misalignment error

Fig. 15 shows that the surface error induced by the ogive effect due to tool misalignment is the most significant one among the ones considered. Since such effect can be assessed and corrected in later iterations of the manufacturing process, it is interesting to see how well the model fits

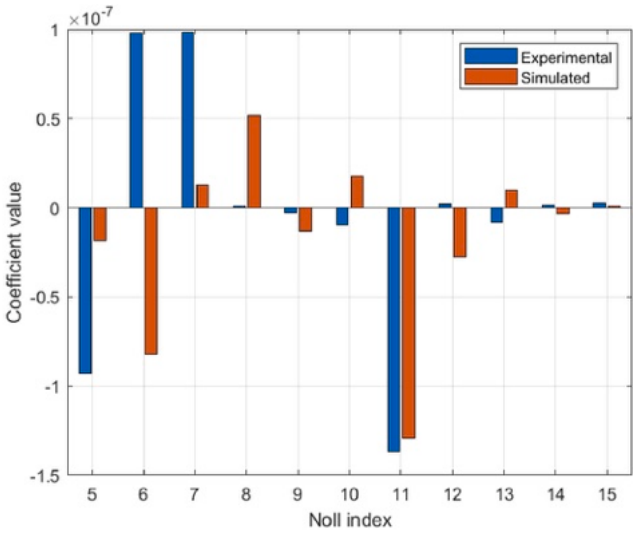

Fig. 20. Zernike coefficients: experimental (blue), simulated (red). (For interpretation of the references to colour in this figure legend, the reader is referred to the Web version of this article.)

the experiment when such effect is removed.

Such removal, however, is not trivial to do in post-processing. In fact, it is not possible to exactly know the relative orientation and position of the ogive with respect to the measurement set-up of the interferometer (i.e., its sphere and optic axis position) as it is in general different from the one of the machine set-up. The best way to evaluate this aspect would be to measure the piece after the misalignment is corrected. This was impossible for the case study, so a numerical manipulation of the results has been carried out, thus intrinsically carrying some error.

The updated deformation maps are shown in Figs. 21 and 22.

The numerical removal of the misalignment effect highlighted some flaws in the prediction, which was already hinted by the mismatching of some Zernike polynomials. While there are similarities among the two maps, it is clear that some additional work has to be done when aiming for a more accurate representation of all the sources of error present in the SPDT process.

Some of the possible improvements to the model include.

- The implementation of the effect of coupling tolerances.
- A more accurate modeling of the tool misalignment effect (i.e. ogive), e.g., including tool radius.

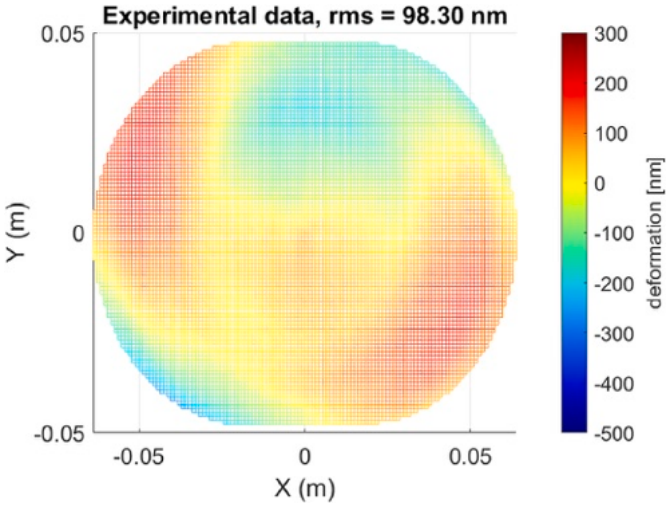

Fig. 21. Experimental results, removed ogive.

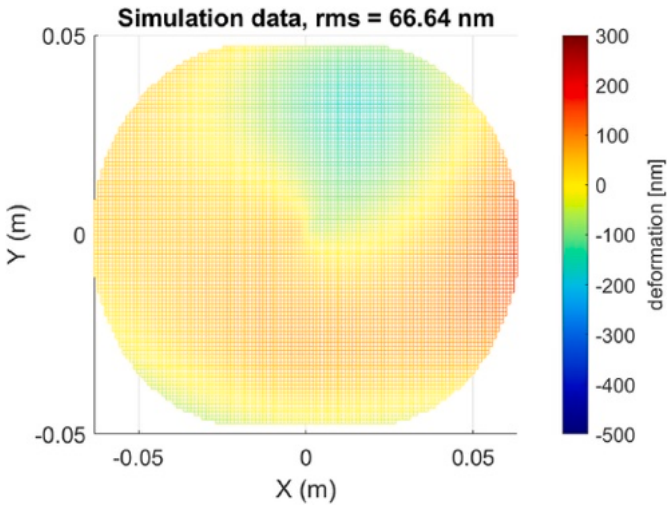

Fig. 22. Simulation results, removed ogive.

- Additional investigation on potential stress induced by the machining process.

5. Conclusions

This work presents a tailored approach for the prediction of SPDT error on optical components, both in terms of deformation and optical aberration.

The following conclusions can be drawn.

- Most of the relevant contributors to manufacturing errors have been included in the methodology.
- A good representativity of the approach was verified by applying it to a case study. The predicted surface represented the experimental one with an error of 1.4 % RMS.
- The evaluation of the Zernike coefficients of the surface performed in the proposed methodology proved to be able to identify the most relevant optical aberrations of the surface as well as correctly predicting the single most significant one.
- Some improvement on the model is, however, needed for the correct estimation of the result of the manufacturing. Such need was as highlighted by both the evaluation of the Zernike polynomials and the removal of the ogive error.

Even with its approximations, the presented approach proved to be well suited to represent the effects of manufacturing during SPDT operations, especially in terms of overall deformation. This presents useful application possibilities as it allows to have an idea of the obtained surface before going to the machine tools, allowing for improvement and optimization of the operations.

In particular, a possible future application of the methodology proposed would be the development of an optimization procedure of the manufacturing process in terms of fixturing and toolpath based on the prediction obtained by applying the approach presented in this paper.

CRediT authorship contribution statement

Daniele Gottini: Writing – original draft, Validation, Methodology, Conceptualization. **Giovanni Scimia:** Writing – review & editing, Validation, Resources, Conceptualization. **Niccolò Grossi:** Writing – review & editing, Methodology. **Antonio Scippa:** Supervision, Project administration, Conceptualization.

Data availability statement

No data are available but can be provided upon request.

Funding

The research received no external funding.

Declaration of competing interest

The authors declare that they have no known competing financial interests or personal relationships that could have appeared to influence the work reported in this paper.

References

[1] Beigmoradi S, Vahdati M. Experimental and numerical study of polishing of 2024 aluminum alloy using acoustics energy. J Manuf Process Jan. 2022;73:440–53. https://doi.org/10.1016/j.jmapro.2021.11.009.
[2] He X, Jin H, Zhou C, Gao C, Zhang G, E S. Modeling of material removal in magnetic finishing based on Maxwell's stress tensor theory and its experimental validation. J Mater Process Technol 2023;312(Mar). https://doi.org/10.1016/j.jmatprotec.2022.117808.
[3] Chabot T, Brousseau D, Auger H, Thibault S. Sub-assembly fabrication of diamond-turned aluminum image slicers. SPIE-Intl Soc Optical Eng; Oct. 2021. p. 52. https://doi.org/10.1117/12.2601142.
[4] Chabot T, Brousseau D, Auger H, Thibault S. Diamond turning of aluminum image slicers for astronomical applications. SPIE-Intl Soc Optical Eng; Nov. 2019. p. 86. https://doi.org/10.1117/12.2536870.
[5] Yu DP, Hong GS, Wong YS. Profile error compensation in fast tool servo diamond turning of micro-structured surfaces. Int J Mach Tools Manuf Jan. 2012;52(1):13–23. https://doi.org/10.1016/j.ijmachtools.2011.08.010.
[6] Li LH, Yu NH, Chan CY, Lee WB. Al6061 surface roughness and optical reflectance when machined by single point diamond turning at a low feed rate. PLoS One Apr. 2018;13(4). https://doi.org/10.1371/journal.pone.0195083.
[7] "1-Rozelot-Aluminum mirror versus glass mirrors".
[8] Pace E, et al. The telescope assembly of the Ariel space mission. Proc SPIE-Int Soc Opt Eng 2022. https://doi.org/10.1117/12.2629432.
[9] Kant G, Sangwan KS. Predictive modelling and optimization of machining parameters to minimize surface roughness using artificial neural network coupled with genetic algorithm. In: Procedia CIRP. Elsevier B.V.; 2015. p. 453–8. https://doi.org/10.1016/j.procir.2015.03.043.
[10] Deshpande K, et al. Manufacturing Line Ablation, an approach to perform reliable early prediction. In: Procedia computer science. Elsevier B.V.; 2024. p. 752–65. https://doi.org/10.1016/j.procs.2024.01.075.
[11] Huang P, Lee WB. Cutting force prediction for ultra-precision diamond turning by considering the effect of tool edge radius. Int J Mach Tools Manuf Oct. 2016;109:1–7. https://doi.org/10.1016/j.ijmachtools.2016.06.005.
[12] Dai Y, Zhang G, Luo T, Luo Q. Centre cone generation and its force performance in single-point diamond turning. Int J Mech Sci Oct. 2020;184. https://doi.org/10.1016/j.ijmecsci.2020.105780.
[13] Craig M, Rank G, Hobson Inc T. "Optical tolerancing for diamond turning ogive error,". 1989.
[14] Zhang J, Zhang X, Tan S, Xie X. Design and manufacture of an off-axis aluminum mirror for visible-light imaging. Current Optics and Photonics Aug. 2017;1(4):364–71. https://doi.org/10.3807/COPP.2017.1.4.364.
[15] Hao X, Li Y, Chen G, Liu C. 6+X locating principle based on dynamic mass centers of structural parts machined by responsive fixtures. Int J Mach Tools Manuf Feb. 2018;125:112–22. https://doi.org/10.1016/j.ijmachtools.2017.11.006.
[16] Mori K, Matsubara A. Estimation of supporting fixture receptance for thin-walled milling. CIRP Annals Jan. 2022;71(1):333–6. https://doi.org/10.1016/j.cirp.2022.04.038.
[17] Calabrese M, Primo T, Del Prete A. Optimization of machining fixture for aeronautical thin-walled components. In: Procedia CIRP. Elsevier B.V.; 2017. p. 32–7. https://doi.org/10.1016/j.procir.2017.02.008.
[18] Raghu A, Melkote SN. Analysis of the effects of fixture clamping sequence on part location errors. Int J Mach Tools Manuf Mar. 2004;44(4):373–82. https://doi.org/10.1016/j.ijmachtools.2003.10.015.
[19] Landwehr M, Kalocsay R, Kolvenbach C, Ganser P, Bergs T. Preparation of Papers for IFAC Conferences & Symposia: adaptive fixture system for reducing machining distortion caused by residual stresses in milling. In: IFAC-PapersOnLine. Elsevier B.V.; 2022. p. 264–9. https://doi.org/10.1016/j.ifacol.2022.04.204.
[20] Moroni G, Petró S, Polini W. Robust design of fixture configuration. In: Procedia CIRP. Elsevier B.V.; 2014. p. 189–94. https://doi.org/10.1016/j.procir.2014.03.120.
[21] Bejlegaard M, ElMaraghy W, Brunoe TD, Andersen AL, Nielsen K. Methodology for reconfigurable fixture architecture design. CIRP J Manuf Sci Technol Nov. 2018;23:172–86. https://doi.org/10.1016/j.cirpj.2018.05.001.
[22] Yip WS, To S. Preliminary investigation on ultra-precision diamond turning of titanium alloys using thermoelectric cooler fixture. J Manuf Process Oct. 2020;58:187–92. https://doi.org/10.1016/j.jmapro.2020.08.020.

[23] Gottini D, et al. FEA testing the pre-flight ariel primary mirror. Proc SPIE-Int Soc Opt Eng 2022. https://doi.org/10.1117/12.2629815.
[24] Tozzi A, et al. Toward ARIEL's primary mirror. Proc SPIE-Int Soc Opt Eng 2022. https://doi.org/10.1117/12.2628906.
[25] Lakshminarayanan V, Flece A. "Erratum: Zernike polynomials: a guide. J Mod Opt 2011;58(7). https://doi.org/10.1080/09500340.2011.633763. 545-561)," Oct. 20, 2011.
[26] Noll RJ. Zernike polynomials and atmospheric turbulence. J Opt Soc Am 1976;66 (3):207–11. https://doi.org/10.1364/JOSA.66.000207.
[27] Malacara D. Optical shop testing. Third Edition; 2006. https://doi.org/10.1002/9780470135976.
[28] Chandra Bhagat K, Kumar Soren S, Chaudhary SK. Experimental and numerical analysis of different aerodynamic properties of circular cylinder. International Research Journal of Engineering and Technology 2016. Available: www.irjet.net.
[29] ESA-ESTEC requirements and standard division. ECSS-E-HB-32-23A-Rev 2023;1.
[30] Nassar SA, Abboud A. An improved stiffness model for bolted joints. J Mech Des 1990;131(12):1210011–12100111. https://doi.org/10.1115/1.4000212. 2009.
[31] Hartung J, Beier M, Peschel T, Gebhardt A, Risse S. Mechanical design implementation and mathematical considerations for ultra precise diamond turning of multiple freeform mirrors on a common substrate. In: Optical systems design 2015: optical fabrication, testing, and metrology V. SPIE; Sep. 2015. 96280U. https://doi.org/10.1117/12.2191043.
[32] Wang Y, Xie F, Ma S, Dong L. Review of surface profile measurement techniques based on optical interferometry. Elsevier Ltd.; Jun. 01, 2017. https://doi.org/10.1016/j.optlaseng.2017.02.004.